Advances in Geosciences Konstantinos Perakis & Athanasios Moysiadis, Editors
EARSeL, 2012

Study of Uncertainties from Evapotranspiration Models Applied to Landsat Data Over a Mediterranean Agricultural Region

Maria Mira[1,2,3], Dominique Courault[1,2], Albert Olioso[1,2], Olivier Hagolle[4], Olivier Marloie[1,2], Sergio Castillo-Reyes[1,2] and Belén Gallego-Elvira[1,2]

[1]*INRA, UMR 1114 EMMAH, F-84914 Avignon, France*

[2]*Université d'Avignon et des Pays de Vaucluse, UMR 1114 EMMAH, F-84000 Avignon, France*

[3]*University of Valencia, Department of Earth Physics and Thermodynamics, C/ Dr. Moliner 50, 46100 Burjassot, Spain*

[4]*CESBIO, BPI 811, 18 Avenue E. Berlin, 31401 Toulouse Cedex 9, France*

maria.mira@avignon.inra.fr

Abstract. A large variety of methods have been developed to retrieve surface energy fluxes, in particular evapotranspiration (ET) from remote sensing data. As a lot of satellites provide a large amount of images at various spatial and temporal resolutions, it is necessary to evaluate the methods frequently used for ET mapping, as well as the methodologies used to estimate the input variables (albedo, surface temperature, emissivity, net radiation, LAI, NDVI). The work presented here aims to assess the modelling of uncertainties in ET estimations from multispectral data. Particular emphasis is given to albedo estimation and 24 different models are being tested from a Landsat-7 dataset. It was acquired over the Crau-Camargue region, located in South Eastern France, between 2007 and 2010. In parallel to these images, continuous ground measurements of albedo, land surface temperature (LST) and surface fluxes are acquired for the same period for different surfaces, including irrigated and dry grassland, natural vegetation and various crops. The results show that each albedo model shows a quite large error (>11%) when compared with ground measurements. Performances are different according to the site upon study and the spectral band considered. The comparison between the different albedo models shows that those are lower over coefficients sets that include the middle infrared bands. Despite these errors, it appears that according to the reliability of albedo estimation ($RMSE_R$=11%), it is possible to retrieve latent heat flux estimates with an uncertainty around 10 $W \cdot m^{-2}$ (ranging from -20 to 25 $W \cdot m^{-2}$).

Keywords. Albedo, surface temperature, net radiation, latent heat flux, emissivity, surface fluxes, remote sensing, Landsat, uncertainties.

1. Introduction

The knowledge of actual evapotranspiration (ET) from soil and crop surfaces is of great importance for agricultural and hydrological studies. However, there are difficulties in measuring or estimating it accurately at regional scale. The close dependence of surface temperature (Ts) on ET rate makes thermal remote sensing well suited to ET mapping.

During the past decades, a large variety of methods have been developed to retrieve surface energy fluxes, in particular ET, from remote sensing data, which are of great interest in meteorology, climatology and hydrology. New missions like the Landsat Data Continuity Mission, Sentinel-2 and Venμs are planned, which will provide data at finer spatial and temporal scales, more suitable than present platforms for monitoring crop water use. In order to use these new data for operational applications, it is necessary to evaluate the methods frequently used for ET mapping, as well as the

methodologies used to estimate the inputs variables (albedo, surface temperature, emissivity, net radiation, LAI, NDVI).

Daily ET is an important variable which allows crop monitoring and water. The cumulated ET through the whole phenological cycle is also closely related to the crop of final productivity. Several papers report on the State-of-the-Art in the field of ET mapping from remote sensing data, underlying their respective advantages and shortcomings [1], [2], [3], [4], [5], [6], [7]). It appears that reliable ET estimates can be obtained from remote sensing information, which makes it possible to provide useful spatially-distributed information on ET over large areas.

A prototype of the processing chain called "EVApotranspiration Assessment from SPAce" (EVASPA) has been developed at the INRA (French National Institute for Agricultural Research) in Avignon to assess daily ET using different models from remote sensing data, at both high temporal resolution with the Moderate Resolution Imaging Spectroradiometer (MODIS) sensor and fine spatial resolution with the Thematic Mapper (TM), Enhanced TM Plus (ETM+) and Advanced Spaceborne Thermal Emission and Reflection Radiometer (ASTER) sensors. This work was made through different projects funded by CNES (TOSCA) and the European SIRRIMED FP7 project. An important dataset was acquired on the Crau-Camargue and Avignon region, located in the South Eastern France, including 29 Landsat-7 images between 2007 and 2010 and a large set of ground measurements performed for various surfaces.

We therefore focused here on analyzing different algorithms for the assessment of biophysical variables and ET derived from Landsat-7 images, with particular emphasis on algorithm dedicated to albedo estimates. Emerging as a continuation of previous work [8], a target calibration procedure for obtaining surface albedo from Landsat-7 data is presented here. To better understand this choice, it is important to point out that albedo has been chosen as the first variable to be analyzed, because it is among the main variables occurring in all exchanges between the surface and the atmosphere. Albedo is mandatory for local and regional estimates of energy and mass exchanges between the Earth surface and the atmosphere, since it determines the quantity of solar radiation which is absorbed by the Earth surface. It provides information on the radiative balance and thus on available energy for ET. Albedo represents the amount of solar energy reflected by the surface and is a dimensionless biophysical characteristic of the soil-plant canopy system over lands. It is expressed as the ratio of the radiant energy scattered upward by a surface in all directions, compared to that received from all directions (direct and scattered by the atmosphere solar radiation), integrated over the wavelengths of the solar spectrum [9]. Albedo depends on the irradiance conditions and thus varies constantly throughout the day [10] and the year.

The paper is structured as follows: after a brief presentation of the experimental site and data, the approach used to estimate ET and the different albedo models evaluated, is presented. Next, the estimations of albedo and net radiation obtained from Landsat-7 data compared to ground measurements are presented. Finally, the impact of error in albedo estimation on uncertainties in deriving net radiation and ET is analyzed.

2. Materials

2.1. The experimental sites

The study region is located in the lower Rhône Valley, South Eastern France, including the Avignon area (43.92°N; 4.88°E; 32 m above sea level) and the "Crau–Camargue" area (43.53°N; 4.66°E; 3 m above sea level). It is a flat area which presents a wide variety of surfaces including dry and irrigated grasslands, and various crops. Climate is typically Mediterranean, with irregular precipitations, long dry periods in spring and summer, and strong winds.

2.2. Ground based measurements

A large ground measurement network has been deployed in Crau-Camargue and the INRA research center in Avignon (Figure 1), by the EMMAH INRA unit, to automatically monitor the meteorological variables as well as the energy surface fluxes (Figure 1). An important dataset (Table. 1) is thus available on various surfaces including albedo and net radiation measurements. Turbulent flux measurements were also performed with eddy covariance systems (latent and sensible heat fluxes) but not used in the present study.

Table 1. Summary of the sites and ground measurements used for this study.

Site name	Characteristics	Measured variables	Period
Avignon	Various crops	Albedo (α) Surface brightness temperature (Tb) Net radiation (Rn)	2007-2010
Coussouls	Natural vegetation		2007-2010
Merle	Irrigated grassland		2009-2010
Tour du Valat	Salty marshes		2010

Net radiation was measured with an accuracy of 5% to 10% with four components pyradiometers (Kipp and Zonen CNR1) mounted between 1.5 m and 2 m above canopy top. The radius of the measurement footprint ranged from around 25 to 35 m. Albedo was obtained from the two pyranometers components of the CNR1 instrument measuring radiation over the whole solar spectrum (300 to 3000 nm). Measurements were averaged over 30 minute periods. Surface brightness temperature (Tb) was derived from upward longwave radiation measurements from CNR1 instruments.

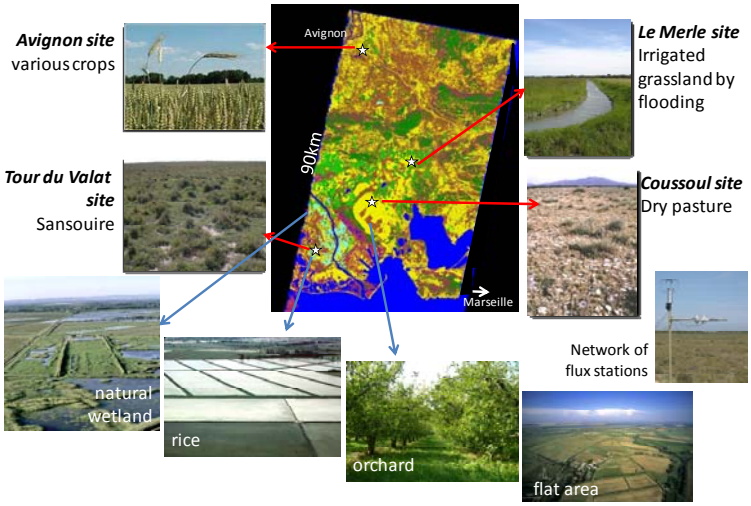

Figure 1: The "Crau-Camargue" and lower Rhône Valley study area, South Eastern France. Location of the main sites used for this study, where albedo, net radiation and convective fluxes were measured.

2.3. Landsat-7 data

The Earth observation satellite Landsat-7 Enhanced Thematic Mapper Plus (ETM+) is in sun-synchronous orbit about 705 km above the Earth and collects data in a swath of 185 km. Its revisit interval is 16 days. The ETM+ bands 1 through 5 and 7 are 30 × 30 m spatial resolution. The thermal infrared band 6 (10.40–12.50 µm) has spatial resolution of 60 × 60 m (for more details see *landsat.gsfc.nasa.gov/about/etm+.html*).

In the present study, we used a data set of 29 Landsat-7 ETM+ images acquired between 2007 and 2010 over the lower Rhône Valley including the Crau-Camargue region at 10:21 UTC. These data were downloaded via the *http://glovis.usgs.gov* platform and then corrected for geolocation and atmospheric effects in *Center for the Study of the Biosphere from Space* (CESBIO) at Toulouse

(France) according to the method described by [11] and [12]. Because of a technical problem on the sensor, as described on the Landsat web site, only the central part of the scene is to process (44 x 90 km). The study site was targeted with a viewing angle around 15° close to nadir.

3. Methods

3.1. Evapotranspiration mapping

The main steps of the processing chain EVASPA developed to map biophysical variables and surface fluxes from Landsat data are illustrated in Figure 2.

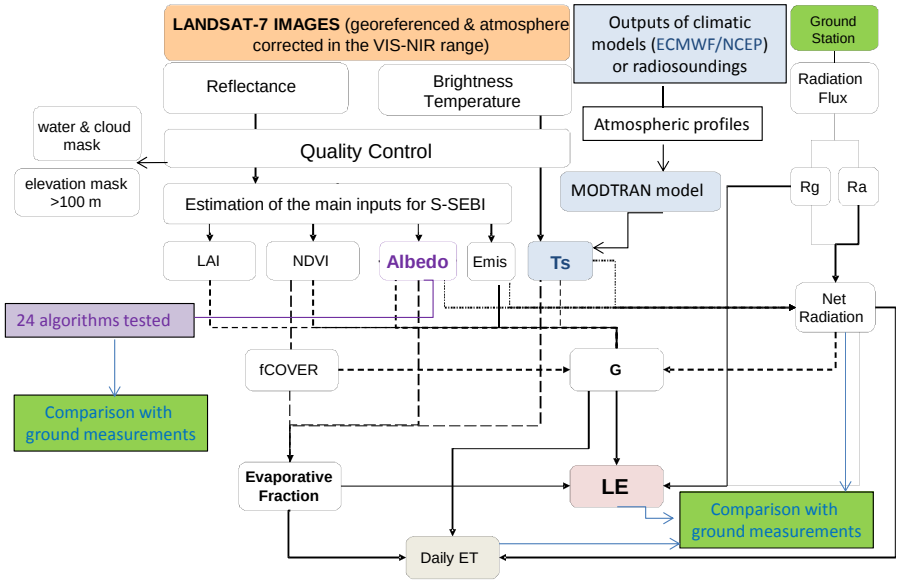

Figure 2: Diagram describing the algorithms to map daily ET from Landsat as being set for the EVASPA tool. LAI: leaf area index; NDVI: normalized difference vegetation index; Emis: emissivity; Ts: surface temperature; fCOVER: fraction cover; G: ground heat flux; LE: latent heat flux; ET: evapotranspiration; Rg: short wave incoming radiation; Ra: long wave incoming radiation.

Among the different ET models proposed in literature, the Simplified Surface Energy Balance Index model (S-SEBI) [13] was chosen, because it is easy to implement for operational applications. It is based on a contextual method (albedo, α, versus radiative surface temperature, Ts), to estimate the ratio of ET to available energy (called evaporative fraction). In addition to albedo and surface temperature, only incident radiation data are required. No additional meteorological data, such as wind speed and air temperature, are needed, neither surface roughness variables. Contextual methods significantly reduce the impact of errors on the determination of surface temperature on the estimation of ET and greatly improve the robustness of the estimates [14]. The determination of wet and dry limits, inferred from the spatial variability found in the remote sensing images, is necessary to compute the latent heat flux (LE) from the evapotranspiration fraction (EF) following Equation 1:

$$LE = EF\ (Rn - G) \quad (1)$$

where Rn and G are the net radiation and soil heat flux, respectively. NDVI, albedo, emissivity (ε) and surface temperature (Ts) were derived from remote sensing data using empirical relationships. Rn was computed as defined by Equation 2:

$$Rn = (1 - \alpha)\ Rg + \varepsilon\ Ra - \varepsilon\ \sigma\ Ts^4 \quad (2)$$

where Rg and Ra are the short and long wave incoming radiation, respectively, and σ the Stefan-Boltzmann constant.

Albedo (α) appears as a key variable in this approach, as well as the surface temperature. Thus, a special attention is focused on the estimation of these two variables. Ts was obtained from the thermal Landsat band 6. The atmospheric radiative transfer model MODTRAN® [15] was used to remove the atmospheric effect on the band 6 using atmospheric profiles obtained from either in situ radiosoundings made at Nimes (30 km Western of the Landsat scene), or from climatic models (*European Centre for Medium-Range Weather Forecasts*, ECMWF, or the *National Centers for Environmental Prediction*, NCEP). The results (not displayed here) have shown that the impact of the variability of these atmospheric profiles on the estimation of the surface brightness temperature (Tb) can be considered as negligible since they induce non-significant errors on Tb. Tb were then compared to ground measurements. Accuracy was in the order of 1.9 K, which was acceptable compared to values found in literature. Then emissivity was derived using the formula proposed by [16]. Finally, the radiative surface temperature Ts was computed from Tb according to the model described in [17].

For albedo estimation, several models were considered for comparison and validation over the Crau-Camargue dataset, as described in the following section.

3.2. Albedo algorithms

This work arises as a continuation of previous work [8] in which albedo was computed from Landsat-7 data following 12 different models from literature [18], [19], [20], [21], [22], [23], [24]. This paper presents a study completing this work by providing new albedo models more suitable for our study site and sensor. Thus new models using various combinations of wavebands from ETM+ were calibrated over the area using ground measurements of albedo over various land surfaces. The contribution of each spectral band to albedo estimation is discussed in the result section.

Simple models were chosen for the analysis. They are based on linear combination of reflectances (ρ) from different spectral bands with various coefficient dataset as specified by Equation 3:

$$\alpha = \beta_0 + \sum_{j=1}^{n} \beta_j . \rho_j \tag{3}$$

where j corresponds to a specific spectral band among the n spectral bands, β_j are the coefficients to be adjusted, and β_0 is the offset. Table 2 summarizes the 12 sets of coefficients from literature tested. The algorithms from [18] and [19] were defined to derive albedo from Landsat-5 TM imagery. The formula proposed by [20] was devoted to the MISR sensor, and calibrated over a simulated dataset by considering nadir bidirectional reflectances. The weighting coefficients based on at-surface solar radiation proposed by [21] were derived as an operational method for estimating albedo applicable to Landsat satellite sensors for typical cloud-free, low-haze conditions and sensor view angles less than 20°. The set from [22] was calibrated over the Crau–Camargue dataset using FORMOSAT-2 off nadir bidirectional reflectances. Algorithms defined by [23] were calibrated over a simulated dataset and designed for hemispherical reflectances collected within generic wavebands: I – NOAA, II – MSG, III – MISR/MERIS. And finally, coefficients from [24] were calibrated over a measured dataset, and designed for nadir (set 1, 2 and 3) and hemispherical (set 4) reflectances collected within airborne PolDER wavebands.

To consistently calibrate and validate the empirical methods we considered to estimate albedo. It was necessary to perform spatial and temporal matching between ground based and satellite data, and mask water and clouds from Landsat acquisitions. An interpolation between albedo values acquired at 10:15 and 10:45 UTC was made to obtain an estimate of albedo matching Landsat-7

overpasses at 10:21 UTC. The resulting dataset included 70 ground samples coincident with Landsat acquisitions.

New models were derived from ETM+ images and albedo ground data. Equation 3 was calibrated using multiple linear regression between spectral reflectances and albedo (MATLAB function called *regress*). Different combination of spectral reflectances were tested giving a new set of albedo models (labeled as a13 to a24), making it possible to analyze the influence of each spectral band in the calculation of albedo. The weighting coefficients and the regression performance for each model are given in the next section.

Table 2. Coefficients sets used to compute albedo as a linear combination of waveband Landsat-7 reflectances. βo is the offset and $\Sigma\beta_i$ corresponds to the sum of coefficients (except β_0). The sensor for which each model was originally defined is also presented. NIR: near infrared; MIR: middle infrared.

	Albedo algorithm	*Sensor*	*Blue (b1)*	*Green (b2)*	*Red (b3)*	*NIR (b4)*	*MIR1 (b5)*	*MIR2 (b7)*	β_0	$\Sigma\beta_i$
(a1)	Duguay & Ledrew (1992)	Landsat-5	–	0.526	–	0.3139	–	0.112	–	0.9519
(a2)	Dubayah (1992)	Landsat-5	0.221	0.162	0.102	0.354	0.059	0.0195	–	0.9175
(a3)	Liang et al. (1999)	MISR	–	0.126	0.343	0.415	–	–	0.004	0.884
(a4)	Tasumi et al. (2008)	Landsat	0.254	0.149	0.147	0.311	0.103	0.036	–	1.000
(a5)	Bsaibes et al. (2009)	FORMOSAT-2	–	–	0.619	0.402	–	–	–	1.021
(a6)	Weiss et al. (1999) – I	NOAA	–	–	0.570	0.460	–	–	–	1.030
(a7)	Weiss et al. (1999) – II	MSG	–	0.680	0.080	0.350	–	–	–	1.110
(a8)	Weiss et al. (1999) – III	MISR/MERIS	0.06	0.69	0.001	0.35	–	–	–	1.101
(a9)	Jacob & Olioso (2002) set1		–	–	0.2268	0.3055	–	–	0.0595	0.5323
(a10)	Jacob & Olioso (2002) set2	Airborne	–	-0.1355	0.3339	0.3162	–	–	0.0588	0.5146
(a11)	Jacob & Olioso (2002) set3	PolDER	-0.0992	-0.0869	0.3509	0.3137	–	–	0.0579	0.4785
(a12)	Jacob & Olioso (2002) set4		–	–	0.591	0.374	–	–	-0.001	0.965

Performances were assessed using standards metrics:

- Mean Error (ME), was the bias between estimated (E_i) and measured (M_i) values (as defined by Eq. 4).

- Absolute Root Mean Square Error ($RMSE_A$) quantified the scatter between measured and estimated values, and Relative Root Mean Square Error ($RMSE_R$) was the ratio of $RMSE_A$ to the mean of measured values ‹M_i› (as defined by Eq. 5 and Eq. 6).

$$ME = \frac{1}{n}\sum_{i=1}^{n}\left(Estim_i - Meas_i\right) \tag{4}$$

$$RMSE_A = \sqrt{\frac{1}{n}\sum_{i=1}^{n}\left(Estim_i - Meas_i\right)^2} \tag{5}$$

$$RMSE_R = \frac{RMSE_A}{mean\left(Meas_i\right)} \tag{6}$$

4. Results and discussion

This section presents the results obtained when retrieving albedo from Landsat-7 data, their comparison with ground data, and finally the impact of albedo reliability on net radiation and latent heat flux estimation. The values of observed albedo (Figure 3a) were within the range of usual values reported in the literature, for both bare soil and vegetation cover conditions, as they ranged from 0.10 to almost 0.26.

4.1. Albedo models calibrated over the ground dataset for Landsat-7 data

Table 3 describes the derived weighting parameters designed for Landsat-7 spectral configuration and calibrated over the Crau-Camargue dataset.

The underlying concept for deriving albedo from narrow band measurements is to divide a spectral reflectance curve into segments of uniform reflectance, each segment being represented by a narrow band measurement [25]. Hence, an accurate albedo value is constructed from these narrow band measurements by a weighted average technique. The weighting factors for each band are then close to the proportion of solar radiation, incident at the Earth's surface, in each segment. Therefore, the sum of coefficients ($\Sigma\beta_j$) should have a value close to one and coefficients should be positive. However, as observed in Table 3, that sum can be high when the blue band was used: a high value was always obtained for coefficient corresponding to the blue band. At the same time negative values were obtained for coefficients corresponding to the green and the red bands. Negative values were also obtained by e.g. Jacob and Olioso (Table 2). In these latter results, the sums of coefficients were also very different from 1.0 and large constant coefficients β_0 were obtained (that should result in unrealistic albedo estimates for dark surfaces). Despite that and the fact that reflectance in blue band can be affected by residual atmospheric contamination effects, its consideration improves albedo estimates of our Mediterranean agricultural region, as discussed in the following section.

Table 3. Weighting coefficients for each considered band obtained from consideration of multiple linear regressions calibrated over the Crau-Camargue dataset, used to compute albedo as a linear combination of waveband Landsat-7 reflectances. $\Sigma\beta_i$ corresponds to the sum of coefficients. NIR: near infrared; MIR: middle infrared.

Albedo algorithm	*Blue (b1)*	*Green (b2)*	*Red (b3)*	*NIR (b4)*	*MIR_1 (b5)*	*MIR_2 (b7)*	$\Sigma\beta_i$
(a13)	–	–	0.5973	0.4031	–	–	1.0004
(a14)	–	0.9252	-0.0827	0.3414	–	–	1.1839
(a15)	1.8271	-0.6736	0.0515	0.3976	–	–	1.6026
(a16)	1.9252	-0.7492	-0.3294	0.3134	0.2973	–	1.4573
(a17)	1.7336	-0.9229	-0.4767	0.3764	-0.0011	0.6144	1.3236
(a18)	–	0.0125	–	0.3672	–	0.4801	0.8597
(a19)	1.7341	-0.9227	-0.4772	0.3761	–	0.6133	1.3236
(a20)	–	0.5852	-0.6194	0.3223	–	0.6308	0.9188
(a21)	1.0107	–	-0.7152	0.3360	–	0.5908	1.2223
(a22)	1.8979	-1.4939	–	0.4148	–	0.4988	1.3176
(a23)	–	–	-0.2633	0.3574	–	0.6901	0.7842
(a24)	–	0.4732	–	0.3109	0.2006	–	0.9847

4.2. Evaluation of albedo estimates from Landsat-7 data with ground measurements

Table 4 display the results obtained for the retrieval of albedo when validating the different coefficients sets proposed (models a1 to a24) with ground data.

As set by [8], performances resulting from evaluation of albedo estimates from models defined for sensors different than Landsat-7 (i.e., Landsat-5, MISR, FORMOSAT-2, NOAA, MSG, airborne PolDER) presented a systematic bias (ME up to -0.023, Table 4). Hence, the need of a calibrated albedo model for Landsat-7 spectral bands was necessary. The systematic bias might be due to differences in spectral bands between Landsat-7 and the other sensors (this assumption will have to be investigated in the future). Another reason may rely on differences in the quality of the data used to calibrate the models (ground measurements or simulation of albedo).

As summarized in Table 3, different models were tested with the purpose to analyze the contribution of each band to albedo estimation. Table 4 indicates that considering only red and NIR

bands (model a13), it was possible to estimate albedo with a $RMSE_R$ around 14%. That corresponded to the best reliability obtained from previous models (a5, a7, a8). However, this corresponded to the lowest performance observed when calibrating the albedo models over our ground dataset. The inclusion of the green band (model a14) did not improve significantly the albedo estimates (probably because the visible range was already accounted by the red band). Nevertheless, the consideration of one MIR band together with the red and NIR contribution (model a23), allowed an improvement of 2% in terms of $RMSE_R$. That means that the inclusion of MIR reflectance to albedo estimation is important, as expected from [8] in which unbiased estimates of albedo with models including MIR (models a1, a2, a4) were the best. Indeed, when including MIR bands in albedo estimations it makes possible to account for the significant part of the solar spectrum over 1.2 μm. MIR reflectances are also considered as providing valuable information on the geometrical structure of the canopy and the optical properties of the underlying soil and to moisture. As set by [25], ignoring the MIR reflectance of vegetated surfaces could result in an erroneously high albedo (additional error up to 0.02). Note as well that when the green band (model a18) was considered together with the NIR band, instead of the red band, almost the same performances were obtained, being slightly better for the second case (a23).

Going further into the analysis, the inclusion of a forth spectral band improved the $RMSE_R$ up to 11.5%, if the MIR band was taken into account (models a20, a21 and a22, but a15). The best results were obtained for albedo model a19 ($RMSE_R$=11.2%), which considered the contribution of five spectral bands, including blue, green, red, NIR and one from MIR (Landsat-7 bands 1 to 4 and 7, respectively). The consideration of the other MIR band (model a16) or both of them (model a17), did not improve the result. It is worth noting that bias values presented for the present models were not zero, but almost negligible (lower than 0.0025).

Table 4. Performances of Landsat-7 estimates of albedo and net radiation of each coefficients set for albedo retrieval in terms of bias (ME), absolute ($RMSE_A$) and relative ($RMSE_R$) Root Mean Square Errors. Standards metrics are associated with the comparison between estimates from Landsat-7 remotely sensed data and ground measurements. Albedo estimates resulting from consideration of offset coefficient β_0 recomputed to correct bias (β_0'= β_0 – ME) are also presented.

	Albedo (α) [Dataset size 70]			*Net radiation (Rn, W·m^{-2})* [Dataset size 67]			*Albedo (α) after unbiasing* [ME(α)=0.000]	
Albedo algorithm	ME	$RMSE_A$	$RMSE_R$ (%)	ME	$RMSE_A$	$RMSE_R$ (%)	$RMSE_A$	$RMSE_R$ (%)
(a1)	-0.023	0.032	17.9	22.7	30.7	7.0	**0.022**	**12.5**
(a2)	-0.022	0.032	18.1	23.0	31.3	7.1	0.023	13.1
(a3)	-0.010	0.028	15.7	14.7	26.6	6.1	0.026	14.6
(a4)	-0.016	0.028	15.5	17.6	27.2	6.2	0.023	12.7
(a5)	**0.000**	0.026	14.5	6.2	**23.5**	**5.4**	0.026	14.5
(a6)	0.010	0.029	16.5	**-0.5**	23.7	5.4	0.027	15.4
(a7)	-0.006	**0.025**	**14.0**	10.8	24.1	5.5	0.024	13.6
(a8)	-0.009	0.026	14.5	13.4	25.3	5.8	0.024	13.4
(a9)	-0.010	0.027	15.2	16.0	29.3	6.7	0.025	14.2
(a10)	-0.009	0.027	15.1	15.5	28.8	6.6	0.025	14.2
(a11)	-0.011	0.028	15.6	16.8	29.5	6.7	0.025	14.3
(a12)	-0.012	0.028	15.6	14.4	26.1	6.0	0.025	14.0
(a13)	-0.0022	0.026	14.4	**8.0**	23.6	5.4		
(a14)	-0.0018	0.025	13.8	8.2	23.2	5.3		
(a15)	-0.0007	0.023	12.9	8.7	23.3	5.3		
(a16)	-0.0005	0.022	12.1	9.0	23.3	5.3		
(a17)	-0.0012	**0.020**	**11.2**	10.3	23.5	5.4		
(a18)	-0.0022	0.023	12.6	9.1	**22.3**	**5.1**		

(a19)	-0.0012	**0.020**	**11.2**	10.3	23.5	5.4
(a20)	-0.0022	0.022	12.2	9.9	22.8	5.2
(a21)	-0.0014	0.020	11.5	10.1	23.4	5.3
(a22)	**-0.0011**	0.021	11.5	9.8	22.8	5.2
(a23)	-0.0025	0.022	12.4	9.9	22.7	5.2
(a24)	-0.0018	0.024	13.4	8.1	22.7	5.2

Figure 3a shows the correlation between Landsat-7 estimations and ground measurements for the albedo model a19 considering all available data. This model presented the best results in Table 4 together with model a17. Actually, these two models were almost equivalent since the MIR_1 band which was not used in model a19 had a negligible role in model a17 (coefficients are very close for both models). The model a19 was considered as preferable because it requires information from one less band. Thus, bias was almost negligible (MA=-0.0012) and $RMSE_R$ was acceptable, close to 11%. The quality of albedo retrieval may be considered as quite good considering the variability of land cover types and of measurement periods included in the analysis. This level of error is in the lower range of error obtained when albedo models were tested against independent (not used for calibration) datasets in several other studies (e.g. [22], [26]). However, the structure of the coefficients set for the model was problematic since the sum of coefficient is not really close to 1.0 and negative coefficients are obtained for the green and the red bands (compensating for the high coefficient value for the blue band).

4.3. Assessment of model uncertainties caused by albedo estimates from Landsat-7 data

The aim of this section is to evaluate the impact of albedo reliability into estimates of net radiation and ET.

If the model with the best performance for net radiation is chosen (algorithm a18 according to Tab. 4), retrieved net radiations show a good estimation with a low bias (ME=9 W/m^2) and a $RMSE_A$ of 22 W/m^2 representing around 5% of the value (Figure 3b).

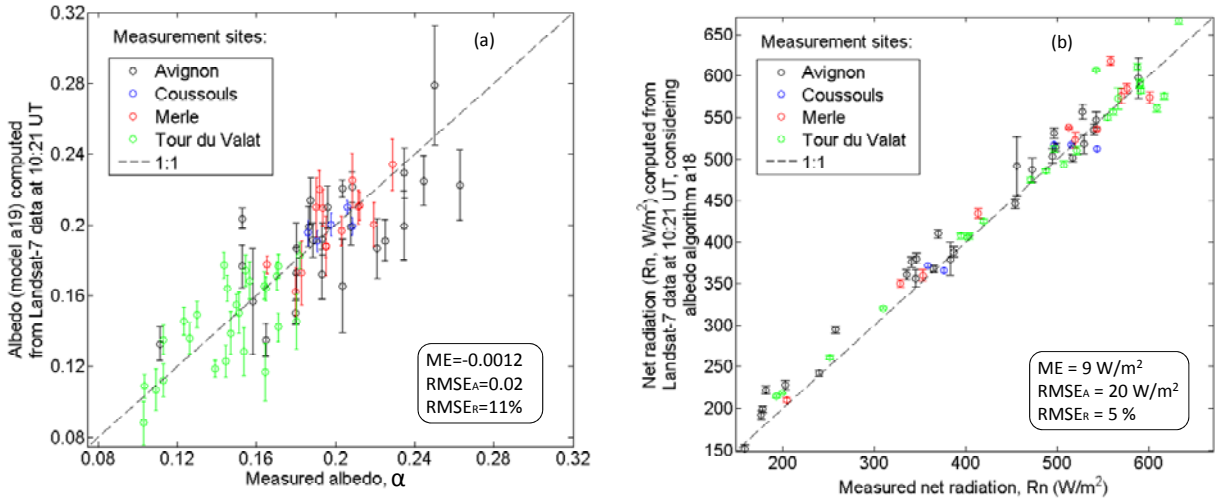

Figure 3: Comparison, over the four measurement sites, between Landsat-7 retrievals and ground based measured (a) albedo and (b) net radiation. Are also indicated the performances in terms of bias (ME), absolute ($RMSE_A$) and relative ($RMSE_R$) Root Mean Square Errors.

Net radiations obtained using the best albedo model were also presenting good matching with ground measurements (model a19) and the use of any of the albedo models calibrated over the ground data resulted in very close values of $RMSE_A$ (all of them lower than 24 W/m^2), showing that the impact of the number of bands in the albedo model is limited on these data. All these values

were lower than the $RMSE_A$ obtained when using almost any of the albedo models from the literature (models a1 to a12). For these last models, the impact of the number of bands was noticeable since the best performances were obtained using the simplest models combining only red and near infrared bands (models a5, a6 and a12) or green, read and near infrared bands (model a8).

In general, net radiations were overestimated, in agreement with albedo underestimations. Relative errors on net radiation were 2 to 3 times lower than relative errors on albedo estimates (Table 4) which was linked to values of absorbed solar radiation at least three time larger than the reflected radiation (albedo lower than ~0.25).

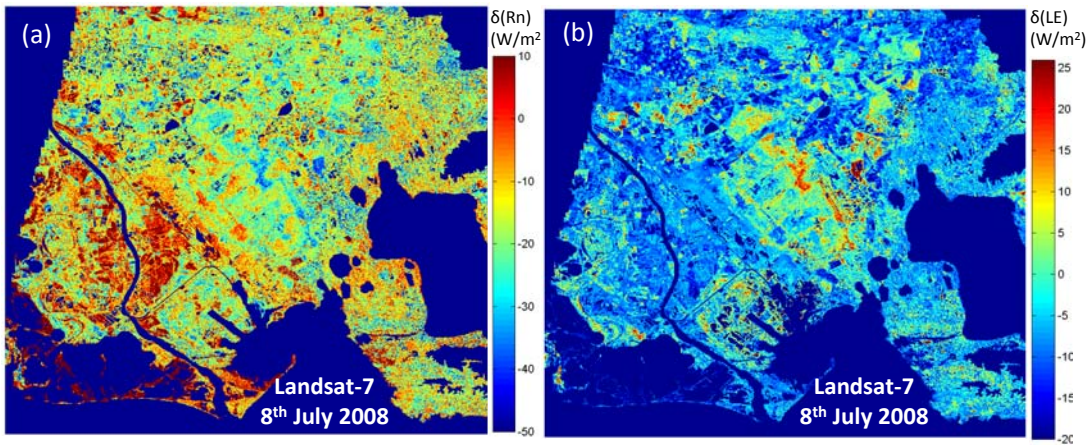

Figure 4: Uncertainties (evaluated as the differences between the best and the worst albedo model) in (a) net radiation, Rn, and (b) latent heat flux, LE (S-SEBI algorithm), estimates resulting from albedo uncertainty over the Crau area on July 8th 2008 from Landsat-7 data. Pixels with δ(Rn) lower than -50 $W \cdot m^{-2}$ and δ(LE) lower than -20 $W \cdot m^{-2}$, which represented less than 0.4% of the Landsat image, were masked to increase the contrast.

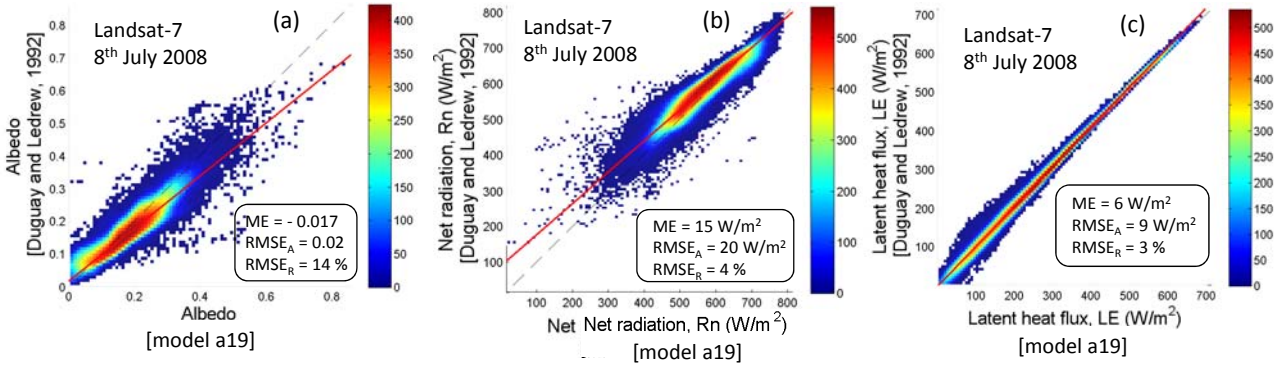

Figure 5: Uncertainty assessment of (a) albedo, (b) net radiation, Rn and (c) latent heat flux, LE (S-SEBI algorithm), estimates resulting from albedo uncertainty over the Crau area on July 8th 2008 from Landsat-7 data.

The expected ranges of uncertainties in net radiation (δ(Rn)) and latent heat flux (δ(LE)) estimates are mapped in Figure 4 for a certain day (8th July 2008). They are computed considering the subtraction between flux estimates from consideration of albedo algorithms a19 and a1 [17], [26] (presenting the best and the worst albedo performances, respectively). This provides, in a way, an assessment of the highest level of uncertainties in the derivation of Rn and LE in relation to error in albedo estimates.

From the analysis of Figure 4, it is observed that globally highest errors belong to either zones close to the border of water bodies, areas with high humidity, such as the irrigated orchards in the coussouls area (Figure 6), or urban areas. The first case could be explained by problems in the water mask definition, and therefore it should be checked in future work. The other cases could be

explained by differences in albedo algorithms (in particular the inclusion of the blue band in model a19, which can be affected by residual atmospheric contamination effects), but further analysis on the matter is required.

The comparison of Landsat-7 estimates of Rn and LE from the pair of considered albedo models (a19 and a1) for one selected day (July 8th 2008) is given in Figure 5bc. The bias between albedo estimates was also observed in net radiation estimates (up to 15 Wm^{-2}) but resulted in a limited difference (20 Wm^{-2}). Large differences mostly affected lowest Rn values which were related to the highest albedo values (urban, quarries) and affected very limited area in the image (Figure 4a) (only 4% of the Landsat scene has $\delta(Rn)<-30$ $W \cdot m^{-2}$). When studying latent heat flux estimates (Figure 5c), this bias disappeared. This is probably explained because the algorithm used to estimate the evaporative fraction [27] considered the limited number of concerned pixels as outliers and drop them for the evaporative fraction analysis (but further analysis is required). Thus, for the presented case, a very good correlation between *LE* estimates from the two different algorithms for albedo estimation is observed (with a bias lower than 6 $W \cdot m^{-2}$ and a very low $RMSE_A$=9 $W \cdot m^{-2}$ ($RMSE_R$=3%)).

4.4. Evapotranspiration estimates from Landsat-7 data

Latent heat flux maps were computed for each Landsat dates with the EVASPA tool. Figure 6 shows the results obtained for 8th July 2008 where we can clearly distinguish the functioning of the different crops and land use. High values (in red) correspond to irrigated grasslands, rice and swamps, whereas dry pasture (coussoul), wheat stubble and orchards present low *LE*.

As an example of temporal evolution, instantaneous latent heat flux maps derived using the algorithm corresponding to S-SEBI, are presented in Figure 7. The image sequence displays the evolution of LE for the various ecosystems in the Crau area and part of the adjacent (West) Camargue area, showing a large variability in terms of water behaviour, in particular in summer when the difference between dry zones, as coussouls area, and wet zones, as irrigated grasslands and marsh areas, is very high.

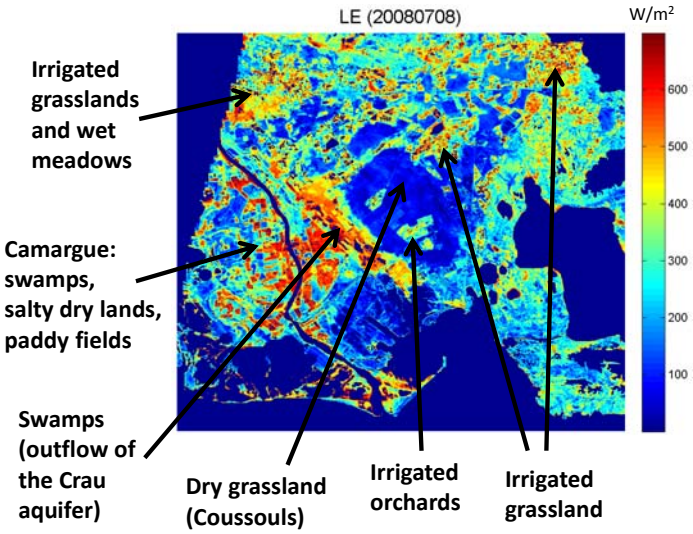

Figure 6: Instantaneous latent heat flux (LE) map obtained from Landsat-7 data over the Crau area on July 8th 2008 using EVASPA (S-SEBI algorithm) showing several areas of interest. Image width is 42 km.

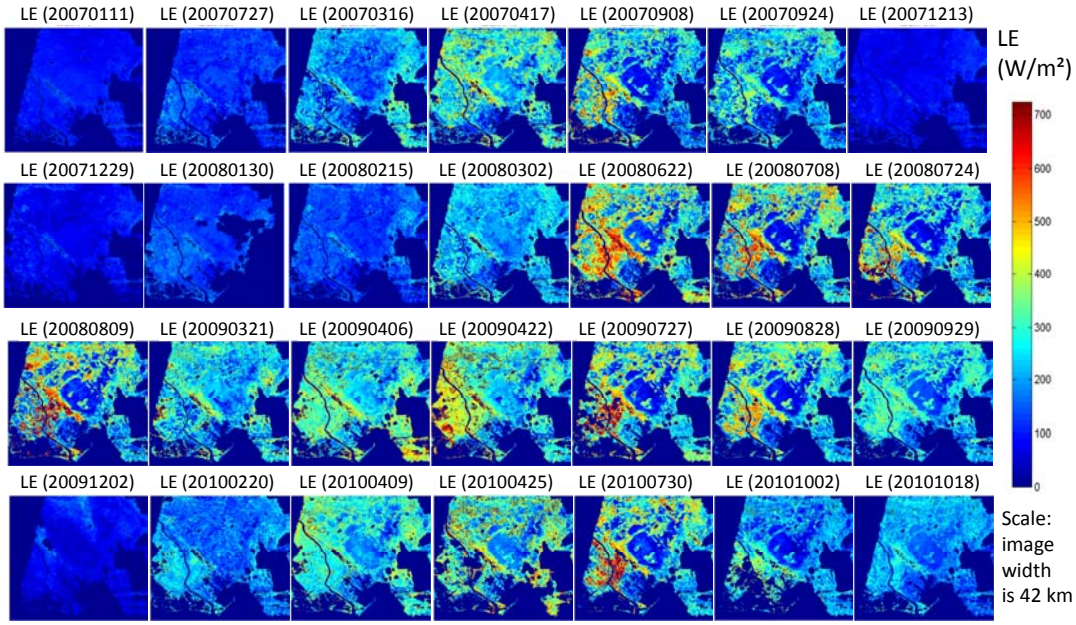

Figure 7: Latent heat flux (LE) maps obtained from Landsat-7 data over the Crau area using EVASPA tool (S-SEBI algorithm). The title of the image gives the acquisition date in the following format LEyyyymmdd.

5. Conclusions

The ET mapping tool (EVASPA developed thanks to fundings from CNES (TOSCA project) and EC FP7 (SIRRIMED projects)) was applied to Landsat-7 data. It allows us to derive high resolution maps of instantaneous latent heat flux over the Crau-Camargue region from albedo and surface temperature derived from satellite images. The analysis of various albedo models through EVASPA demonstrates that the accuracy in albedo estimation is high enough for deriving net radiation and latent heat flux maps with low uncertainties.

The study shows that it is possible to retrieve albedo from Landsat-7 data along with empirical approaches, based on multiple regressions with acceptable errors when considering the derivation of ET. However, a more careful analysis of the albedo model used in this study, in particular of their spectral configuration may lead to potential improvement of albedo estimation.

Indeed, each albedo model shows a significant error (>11%) when compared to ground measurements. Performances are different according to the site upon study and the spectral band considered. Most models overestimate albedo, mostly because of systematic bias (unbiasing estimates strongly improved model performances). It is important to notice that albedo model were developed for various sensors with differences in the design of spectral bands (and in consequence the number of bands used has no real impact on the performances).

Despite these errors, it appears that according to the reliability of albedo estimation ($RMSE_R$=11%), it is possible to retrieve latent heat flux estimates with an uncertainty around 10 $W \cdot m^{-2}$ (ranging from -20 to 20 $W \cdot m^{-2}$).

These results will be useful for future applications in agriculture areas, like Landsat Data Continuity Mission, Sentinel-2, MISTIGRI and Venμs. They also highlight the importance of the thermal data in the different methods. Therefore, it would be important to consider an extension of the spectral bands for future missions, to have land surface temperatures in the processing chains for operational applications (as proposed by CNES with the MISTIGRI mission).

Acknowledgements

This work was made through different projects funded by CNES (TOSCA) and the European SIRRIMED FP7 project. M. Mira was funded by the Vali+D postdoctoral program and B. Gallego-Elvira by the Ramón Areces Foundation.

References

[1] Courault, D., Seguin, B. and Olioso. A., 2005. Review on estimation of evapotranspiration from remote sensing data: From empirical to numerical modeling approaches. *Irrigation & Drainage Systems*, 19, pp. 223-249.

[2] Olioso, A., Inoue, Y., Ortega-Farias, S., Demarty, J., Wigneron, J-P., Braud, I., Jacob, F., Lecharpentier, P., Ottlé, C., Calvet, J-C and Brisson, N., 2005. Future directions for advanced evapotranspiration modeling: assimilation of remote sensing data into crop simulation models and SVAT models. *Irrigation & Drainage Systems*, 19, pp. 377-412.

[3] Carlson, T. N., 2007. An Overview of the "Triangle Method" for Estimating Surface Evapotranspiration and Soil Moisture from Satellite Imagery. *Sensors*, 7, pp. 1612-1629.

[4] Kalma, J. D., McVicar, T. R. and McCabe. M. F., 2008. Estimating Land Surface Evaporation: A Review of Methods Using Remotely Sensed Surface Temperature Data. *Surveys in Geophysics*, 29, pp. 421-469.

[5] Gowda, P.H., Chavez, J. L., Colaizzi, P. D., Evett, S. R., Howell, T. A. and Tolk. J. A., 2008. ET mapping for agricultural water management: present status and challenges. *Irrigation Science*, 26, pp. 223–237.

[6] Li, Z. L., Tang, R. L., Wan, Z. M., Bi, Y. Y., Zhou, C. H., Tang, B. H., Yan, G. J. and Zhang, X. Y., 2009. A Review of Current Methodologies for Regional Evapotranspiration Estimation from Remotely Sensed Data. *Sensors*, 9, pp. 3801-3853.

[7] Petropoulos, G., Carlson, T. N., Wooster, M. J. and Islam, S. 2009. A review of Ts/VI remote sensing based methods for the retrieval of land surface energy fluxes and soil surface moisture. *Progress in Physical Geography*, 33, pp. 224–250.

[8] Mira, M., Courault, D., Hagolle, O., Marloie, O., Castillo-Reyes, S., Gallego-Elvira, B., Lecerf, R., Weiss, M., Olioso, A., 2012. Uncertainties on evapotranspiration derived from Landsat images depending on reliability of albedo input data over a Mediterranean agricultural region. *Sentinel-2 preparatory symposium*. ESA-ESRIN, Frascati (Italy), 23-27 April 2012.

[9] Pinty, B. and Verstraete, M. 1992. On the design and validation of surface bidirectional reflectance and albedo model. *Remote Sensing of Environment*, 41, pp. 155-167.

[10] Kimes, D. S., Sellers, P. J. and Newcomb, W. W., 1987. Hemispherical reflectance variations of vegetation canopies and implications for global and regional energy budget studies. *Journal of Climate and Applied Meteorology*, 26, pp. 959-972.

[11] Hagolle, O., Dedieu, G., Mougenot, B., Debaeker, V., Duchemin, B. and Meygret, A., 2008. Correction of aerosol effects on multitemporal images acquired with constant viewing angles: Application to Formosat-2 images. *Remote Sensing of Environment*, 112, pp. 1689−1701.

[12] Baillarin, S., Gleyzes, J. P., Latry, C., Bouillon, A., Breton, E., Cunin, et al., L., 2004. Validation of an automatic image orthorectification processing. In *IGARSS's Proceedings*, 2, pp. 1398:1401.

[13] Roerink, G. J., Su, Z. and Menenti, M., 2000. S-SEBI: Simple Remote Sensing algorithm to estimate the surface energy balance. *Phys. Chem. Earth* (B), 25(2), pp. 147:157.

[14] Tasumi, M., Trezza, R., Allen, R. G. and Wright, J. L., 2005. Operational aspect of satellite-based energy balance models for irrigated crops in the semi-arid US. *Irrigation and Drainage Systems*, 19, pp. 355-376.

[15] Berk, A., Anderson, G. P., Acharya, P. K., Chetwynd, J.H., Bernstein, L. S., Shettle, E. P., Matthew, M. W. and Adler-Golden, J. H., 1999. MODTRAN 4 Users Manual. Hascom AFB, MA: Air Force Res. Lab. Space Vehicles Directorate.

[16] François, C., Ottle, C. and Prevot, L., 1997. Analytical parameterization of canopy directional emissivity and directional radiance in the thermal infrared. Application on the retrieval of soil and foliage temperatures using two directional measurements. *International Journal of Remote Sensing*, 18(12), pp. 2587-2621.

[17] Olioso A. 1995. Simulating the Relationship between Thermal Emissivity and the Normalized Difference Vegetation Index. International Journal of Remote Sensing, 16, 3211.

[18] Duguay, C. R. and Ledrew, E. F., 1992. Estimating surface reflectance and albedo from Landsat-5 thematic Mapper over rugged terrain. *Photog. Eng. & Remote Sens*., 58, pp. 551–558.

[19] Dubayah, R., 1992. Estimating net solar radiation using Landsat Thematic Mapper and digital elevation data. *Water Resource Research*, 28, pp. 2469–2484.

[20] Liang, S., Strahler, A. H. and Walthall, C., 1999. Retrieval of Land Surface Albedo from Satellite Observations: A Simulation Study. *J. Appl. Meteorol*., 38, pp. 712-725.

[21] Tasumi, M., Allen, R. G. and Trezza, R., 2008. At-Surface Reflectance and Albedo from Satellite for Operational Calculation of Land Surface Energy Balance. *J. Hydrolog. Eng.*, 13(2), pp. 51-63.

[22] Bsaibes, A., Courault, D., Baret, F., Weiss, M., Olioso, A., Jacob, F., Hagolle, O., Marloie, O., Bertrand, N., Desfond, V. and Kzemipour, F., 2009. Albedo and LAI estimates from FORMOSAT-2 data for crop monitoring. *Remote Sensing of Environment*, 113, pp. 716-729.

[23] Weiss, M., Baret, F., Leroy, M., Bégué, A., Hautecoeur, O. and Santer, R., 1999. Hemispherical reflectance and albedo estimate from the accumulation of across-track sun-synchronous satellite data. *Journal of Geophysical Research*, 104, pp. 22221–22232.

[24] Jacob, F. and Olioso, A., 2002. Assessing recent algorithms devoted to albedo estimation using the airborne ReSeDa / PolDER database. *1st Int. Symp. Recent Advances in Quantitative Remote Sens.*, Valencia, Spain, pp. 191-198.

[25] Brest, C. L. and Goward, S. N., 1987. Deriving surface albedo measurements from narrow band satellite data. *International Journal of Remote Sensing*, 8(3), pp. 351-367.

[26] Jacob, F., Olioso, A., Gu, X. F., Su, Z., and Seguin, B., 2002. Mapping surface fluxes using airborne visible, near infrared, thermal infrared remote sensing data and a spatialized surface energy balance model. *Agronomie*, 22, pp. 669-680.

[27] Tang, R., Li, Z. L. and Tang, B. 2010. An application of the Ts–VI triangle method with enhanced edges determination for evapotranspiration estimation from MODIS data in arid and semi-arid regions: Implementation and validation. *Remote Sensing of Environment*, 114, pp. 540:551.